Extended Kalman Filtering for Continuous Volumetric MR-Temperature Imaging

Baudouin Denis de Senneville, Sébastien Roujol, Silke Hey, Chrit Moonen, Mario Ries

Extended Kalman Filtering for continuous volumetric MR-Temperature Imaging

Baudouin Denis de Senneville, Sébastien Roujol, Silke Hey, Chrit Moonen and Mario Ries

***Abstract*—Real time magnetic resonance (MR) thermometry has evolved into the method of choice for the guidance of high-intensity focused ultrasound (HIFU) interventions. For this role, MR-thermometry should preferably have a high temporal and spatial resolution and allow observing the temperature over the entire targeted area and its vicinity with a high accuracy. In addition, the precision of real time MR-thermometry for therapy guidance is generally limited by the available Signal to Noise ratio (SNR) and the influence of physiological noise. MR-guided HIFU would benefit of the large coverage volumetric temperature maps, including characterization of volumetric heating trajectories as well as near- and far-field heating.**

In this paper, continuous volumetric MR-temperature monitoring was obtained as follows: The targeted area was continuously scanned during the heating process by a multi-slice sequence. Measured data and a priori knowledge of 3D data derived from a forecast based on a physical model were combined using an Extended Kalman Filter (EKF). The proposed reconstruction improved the temperature measurement resolution and precision while maintaining guaranteed output accuracy.

The method was evaluated experimentally *ex-vivo* on a phantom, and *in-vivo* on a porcine kidney, using HIFU heating. On the *in-vivo* experiment, it allowed the reconstruction from a spatio-temporally under-sampled data set (with an update rate for each voxel of 1.143 s) to a 3D dataset covering a field of view of 142.5×285×54 mm^3 with a voxel size of 3×3×6 mm^3 and a temporal resolution of 0.127 s. The method also provided noise reduction, while having a minimal impact on accuracy and latency.

***Index Terms*—Magnetic Resonance Imaging, Real time systems, Motion analysis.**

I. Introduction

RECENTLY, real time magnetic resonance (MR) thermometry [1] [2] has evolved into the method of choice for the guidance of non-invasive interventional modalities such as high-intensity focused ultrasound (HIFU) [3]. Non-invasive HIFU ablation of kidney and liver tumors has been demonstrated to be feasible in a clinical environment [4] [5]. The principal role of MR-thermometry for the guidance of HIFU ablations is the continuous monitoring of the thermal intervention for an increased patient safety. MR-thermometry can be used to provide necrosis estimates and thus to determine the therapy endpoint: The cumulative temperature allows computing on-line the deposited thermal dose which, compared to the lethal dose (taken as $43°\mathrm{C}$ during 240 minutes), provides an accurate and immediate prediction of tissue necrosis [6]. Thermometric information can then be used for adaptive ablation strategies, which employ feedback control of the HIFU power and dynamic modifications of the HIFU trajectory [7]: Since a complete destruction of the tumor is required to assure therapeutic success, efficient ablation control strategies are required exploiting both electronic beam steering and mechanical displacements of the HIFU transducer. The feedback control algorithm can either be based on the targeted temperature, as it is required for the use of HIFU in local drug delivery applications [8], or directly on necrosis estimates as is preferable for the direct thermal destruction of tumors [6].

However, although it is well established that MR-imaging can provide data with a high spatial resolution, it is in practice difficult to acquire 3D isotropic image volumes of a larger field of view (FOV) in real time. In general, the precision of real time MR-thermometry for therapy guidance is limited by the available Signal to Noise ratio (SNR) and the influence of physiological motion [9]. As a consequence, the inherent trade-offs in MRI between spatial resolution, volume coverage, and scan time leads for fast MRI often to a sacrifice of spatial resolution and coverage in order to improve the temporal resolution. Several strategies have therefore been proposed for reducing the scan times of a Proton Resonance Frequency (PRF) sequence, such as echo-shifted gradient echo imaging [10], SENSE [11], SMASH [12], UNFOLD [13] or k-t BLAST [14]. However, each method introduces new drawbacks in terms of SNR, spatial and temporal resolution.

Initially, MRI temperature monitoring of sonications has been reported in the kidney as well as in the liver in [15] and [16], respectively. For both studies, the MR-temperature monitoring was achieved in a single slice at an update rate of 3.4 seconds or more. However, for direct retroactive control of the heating device, MR-thermometry should have a high temporal and spatial resolution and allow observing the temperature over the entire target area and the vicinity with a high accuracy and precision. First, both the update time and the latency of the thermal information should preferably be substancially shorter [17]. As a consequence, the employed processing for image reconstruction must be able to complete all computations within the time interval between two suc-

Baudouin Denis de Senneville, Mario Ries and Chrit Moonen are with the Imaging Division, UMC Utrecht, Utrecht, Netherlands, (e-mail: {b.desenneville,m.ries,c.moonen}@umcutrecht.nl).

Baudouin Denis de Senneville, Mario Ries and Chrit Moonen are also with the Laboratory for Molecular and Functional Imaging: From Physiology to Therapy, FRE 3313 CNRS/University of Bordeaux 2, 33076 Bordeaux, France.

Baudouin Denis de Senneville is also with the "Institut de Mathématiques de Bordeaux" (IMB), UMR 5251 CNRS/Université Bordeaux 1/INRIA, F-33400 Talence, France.

Sébastien Roujol is with the Cardiovascular Division, Beth Israel Deaconess, Medical Center, Harvard Medical School, Boston, United States.

Silke Hey is with Philips Healthcare, Best, Netherlands.

Manuscript received ...; revised ...

cessive acquisitions and achieve a short processing latency [18]. Second, an extended spatial coverage is a necessary prerequisite to achieve:

- Retroactive control of volumetric heating strategies, based on temperature or thermal dose measurements in a predefined volumes [7].
- Accurate monitoring of collateral damages such edema induced by the low temperature diffusion close to the skin [19] [20]. Similarly, the important difference of the acoustic impedance of soft tissue and bones results in an important heating of the bones by absorption of the acoustic energy [9].

A recent study reported on-line volumetric MRI thermometry in pig livers with an update rate of 400 milliseconds on a volume limited to 5 slices and a relatively high precision of the temperature estimate (the median value of the standard deviation of the temperature was lower than $2^{\circ}\mathrm{C}$) [21]. To further improve the imaging performances, recent studies investigated the possibility of using Kalman filtering to exploit the physical knowledge of the heating process [22] [23]. In [24], Roujol et al. used an Extended Kalman filter (EKF) to combine measured and model predicted temperature data to achieve a measurement noise reduction. A weighting factor (the Kalman gain) allowed adjusting the confidence between the predictor model and the measured data, and was calculated iteratively based on estimates of the measurement noise and the model covariance [25]. The EKF employed the bio-heat transfer equation (BHTE) as the model predictor and dynamically adapts the model covariance in order to achieve measurement accuracy even in regions where the parameters of the BHTE are not exactly known. Alternatively, sparse sampling approaches in k-space have been proposed, which also exploit the physical knowledge of the heating process [26] to achieve off-line an artefact free reconstruction of 3D MR-temperature maps from under-sampled k-space data using sparse sampling approaches [27] [28].

In the current paper, a continuous volumetric MR-temperature monitoring is obtained from spatio-temporally undersampled thermometric data as follows: The targeted area is continuously scanned during the heating process by a multi-slice sequence. Measured data and a priori knowledge of 3D data derived from a forecast based on a physical model are combined using an EKF. The EKF improves both the temperature measurement temporal resolution and precision while maintaining guaranteed output accuracy. The method was evaluated experimentally on both an *ex-vivo* phantom and an *in-vivo* porcine kidney heated using HIFU, and demonstrated to be compatible with a real-time implementation.

II. METHOD DESCRIPTION

The proposed approach combines temperature measurement obtained from a multi-slice acquisition with a model of temperature transfer as follows:

A. Temperature modeling using the Bio Heat Transfer Equation (BHTE) model

The bio-heat transfer equation (BHTE) was employed as the model for 3D temperature prediction, which includes the applied acoustic power P, a priori knowledge of the absorption rate α, the heat diffusion coefficient D and the perfusion value w [29].

$$\frac{\partial}{\partial t}T\left(\vec{r},t\right)=\alpha.P_{(\vec{r},t)}+D.\nabla^2T_{(\vec{r},t)}-w.T_{(\vec{r},t)} \tag{1}$$

where ∇^2 is the Laplacian operator, and $\vec{r}=(x,y,z)$ is the voxel coordinate. In the implemented model, coefficients P, α, D and w were assumed to be spatially and temporally invariant. The spatial distribution of the acoustic pressure field was determined using an acoustic field simulation based on Rayleigh integration over the active transducer surface. The remaining parameters of the bio-heat transfer equation were calibrated similar to the approach proposed by Mougenot et al. [30]. The temperature modeling with the BHTE was performed using a voxel size matching the reconstructed MR measurements. For this purpose, an integration of the analytic distribution of the acoustic pressure field was individually performed over each voxel in the field of view to obtain temperature prediction matching the sampling of the MR measures.

Computation times were shortened by solving the BHTE in the Fourier domain [31], since the problem can be transformed in Fourier space into a linear differential equation, as follows:

$$\frac{\partial}{\partial t}\widetilde{T}_{(\vec{k},t)}+\left(D.k^2+w\right).\widetilde{T}_{(\vec{k},t)}=\alpha.\widetilde{P}_{(\vec{k},t)} \tag{2}$$

where $\widetilde{T}$, $\widetilde{P}$ denotes the Fourier transform of T and P respectively and k denotes the frequency coordinates in the Fourier domain.

B. Volumetric thermal maps calculation

The discrete solution of the BHTE represents a non-linear model for data prediction in Eq. (2) which was addressed using the EKF formalism [25]. The targeted area was continuously scanned during the heating process by a multi-slice sequence. After a new 2D MRI measurement provides a temperature update T_t^m, the Kalman filter computed, in a first pass, the volumetric temperature prediction V_t^- at time t based on the last reconstructed volumetric temperature V_{t-1} by applying:

$$V_t^-=f\left(V_{t-1},u_{t-1}\right) \tag{3}$$

where f represents the BHTE model, u_{t-1} is the control input parameter which in our case corresponds to the HIFU delivered power at time $t-1$.

Subsequently, the part of the thermometric data in V_t^- which corresponds to the currently acquired slice position, is updated with the measured temperature map T_t^m in order to obtain a mixed thermometric volume V_t^m.

Then, the a priori estimate error covariance P_t^- was computed as follows:

$$P_t^-=A_tP_{t-1}A_t^T+Q \tag{4}$$

where A_t is the Jacobian matrix of partial derivatives of f at (V_{t-1},u_{t-1}), A_t^T denotes the transpose t of A_t, P_{t-1} is the a

posteriori estimate error covariance at instant $t-1$ and Q is the process noise covariance related to the model innacuracy.

In a second pass, the EKF combined both the measured thermometric data, which is contained in V_t^m and the predicted data in V_t^-, in order to obtain the Kalman filtered temperature V_t. For this purpose, a weighting factor, the Kalman gain K_t, allowed to adjust in the acquired slice, the confidence between the employed model and the measured data. The Kalman gain was calculated iteratively and is predominantly influenced by two parameters: the process noise covariance Q and the measurement noise (we note R for the measurement noise covariance that relates to the MR-thermometry precision of the measure). K_t is first updated based on the new a priori estimate error covariance:

$$K_t = P_t H^T \left(H P_t^- H^T + R \right)^{-1} \tag{5}$$

where H relates the model state to the measurement (here H is the identity since the measurements are directly obtained in state space).

Then, the Kalman filtered temperature V_t could be computed from the weighted innovation S_t ($S_t = V_t^m - HV_t^-$) as follows:

$$V_t = V_t^- + K_t S_t \tag{6}$$

whereby S_t is only nonzero at the location of the new thermometric measurements. Finally, the a posteriori estimate error covariance P_t was updated as follows:

$$P_t = (I - K_t H) P_t^- \tag{7}$$

C. Estimation of input parameters for the Kalman filter

The measurement noise R could be determined before the heating process by evaluating the temperature variance in the targeted area on a thermometric dataset in absence of any heating (in this study we assumed R to be spatially and temporally invariant). However, the process noise covariance Q, which characterizes the accuracy of the BHTE model to predict the true temperature evolution, is a priori not known and has shown to vary over time (especially between heat up and cool down period). As shown in [24], this can be achieved using an adaptive EKF (AEKF), where Q is automatically adjusted over time based on a dynamic evaluation of the model accuracy for each new measurement. Based on the assumption that the temperature noise is a white noise centered around the true temperature, it was proposed to evaluate the model accuracy at time t by computing the spatio-temporal sum of the difference between predicted and measured data. In the current study, the model accuracy ϵ_t was evaluated on a voxel-by-voxel basis by computing the temperature bias over a temporal window, as follows:

$$\epsilon_t(x,y,z) = \frac{1}{N} \left| \sum_{i=t-N+1}^{t} \left(V_i^-(x,y,z) - V_i^m(x,y,z) \right) \right| \tag{8}$$

The following heuristic was used to find a map Q minimizing the metric ϵ_t on a voxel-by-voxel basis: A maximum acceptable penalty on the temperature bias (noted $\epsilon_{threshold}$) was chosen. Two states were defined for the Kalman filter:

1) A model covariance $Q(x,y,z) = Q_{min}$ was employed for voxels depicting a model accuracy $\epsilon_t(x,y,z)$ lower than $\epsilon_{threshold}$.
2) $Q(x,y,z) = Q_{max}$ was chosen for $\epsilon_t(x,y,z) > \epsilon_{threshold}$.

A value of 0.1 was defined for Q_{min} in the scope of this study. However, the determination of Q_{max} is of great importance and was defined as the maximal temperature error within the update time between two successive slice updates (which is equal to the repetition time multiplied by the applied power and by the absorption rate).

D. Experimental setup

Continuous volumetric MR-temperature imaging was performed on a clinical Philips Achieva 1.5 T MRI (Philips Healthcare, The Netherlands). Heating was achieved with a Philips Sonalleve HIFU system (Philips Healthcare, Finland), which is integrated into the patient bed of the MR-system.

1) Phantom heating study: MRI guided HIFU heating was performed on a phantom using a PRF sequence which acquires one slice placed in the coronal direction, sweeping continuously through ten positions within the desired observation area (Temporal resolution=0.17 s per position). 1000 slices were acquired using a single-shot EPI sequence (TR=17 ms, TE=11 ms, flip angle=10 °, FOV=76 × 100 × 30 mm^3, voxel size=1.5 × 1.5 × 3 mm^3, which was reconstructed to a voxel size of 0.5 × 0.5 × 3 mm^3 to mitigate partial volume effects). Heating was performed using 50 Watts of electrical power during a period of 30 seconds. The accuracy of the MR thermometry in the heated region was evaluated using the readings of a T-type thermocouple probe as an independent reference.

2) In-vivo heating study: MRI guided HIFU heating was performed *in-vivo* in the kidney of a pig under general anesthesia using a PRF sequence which acquires one slice placed in the coronal direction, sweeping continuously through nine positions within the desired observation area (Temporal resolution=1.143 s per position). Each new acquired slice was used to reconstruct dynamically the volumetric temperature over the observation area, as described in II-B. In addition, the sequence continuously acquires one spatially invariant slice placed in sagittal direction through the heated region (the sagittal slice and coronal slices were acquired in an interleaved fashion). This slice provided an additional temperature measurement with a nine fold increased temporal resolution (i.e. equal to 0.127 s) and was the basis for the calculation of a gold standard temperature with a reduced noise as follows: A temporal temperature averaging was performed on a voxel-by-voxel basis over each new succession of nine maps, which increased the SNR by a factor 3. The control slice was positioned in a sagittal direction several millimeters apart from the focal point, in order to limit the signal perturbation of the sweeped slice. 6000 slices were acquired using a single-shot EPI sequence (TR=63.5 ms per slice, TE=25 ms, flip

angle=35 °, FOV=$142.5 \times 285 \times 54$ mm^3, voxel size=$3 \times 3 \times 6$ mm^3, reconstructed voxel size=$3 \times 3 \times 6$ mm^3).

Heating was performed using 250 Watts of electrical power during a period of 50 seconds. Note that since the kidney was static during the experiment, no correction of motion related temperature errors was required.

3) Implementation: All calculations were performed using a dual processor, INTEL 3.1 GHz Penryn, two cores, 8 GB of RAM. To reduce computation time, the volumetric temperature reconstruction was limited to a region of $32 \times 32 \times 9$ voxels centered on the targeted area. In the scope of this study, the effect of perfusion was neglected ($w = 0$). The heat diffusion evaluated to 0.1 mm^2 s^{-1} for both presented experiments. The absorption rate was evaluated to 0.15 and 0.02 KJ^{-1} for the phantom and the *in-vivo* study, respectively. $N = 10$ was defined so that the temporal window size for the evaluation of the temperature bias ϵ_t covered a duration of a few seconds. $\epsilon_{threshold}$ was set to 1°C for the heuristic adaptation of the model covariance.

III. Results

A. Phantom heating study

Fig. 1 shows an example of temperature maps extracted from a volume reconstructed at the end of the heating process. A significant reduction in measurement noise can be visually observed between the original measured MR-temperature data (the spatio-temporally under-sampled measured MR-temperature maps were reconstructed using a sliding window) and the volumetric AEKF reconstructed temperature data. Fig. 2 shows that, using the reference measurement obtained with the thermocouple probe (indicated by the white arrow in Fig. 1d), the precision of the measurement (i.e the standard deviation of the difference between the red and the black curve) was found to be improved from an initial value of $\pm 2.4\,^{\circ}\mathrm{C}$ with the original data (2a), to $\pm 1.4\,^{\circ}\mathrm{C}$ using the proposed AEKF reconstruction (2b). It can be observed however that the accuracy occasionaly decreased to $5\,^{\circ}\mathrm{C}$ off the true value with the AEKF reconstruction.

B. In-vivo heating study

Fig. 3 shows an example of temperature maps extracted from a volume reconstructed at the end of the heating process. Two typical examples of the temporal temperature evolution obtained in the heated region are reported: A voxel located close to the focal point was selected (referred to as voxel #1), as well as a voxel placed further in the vicinity (referred to as voxel #2). The two voxel locations are indicated in Fig. 3.

To illustrate the influence of the Q value on the reconstructed temperature, we first assumed Q to be spatially and temporally invariant and we fixed a low value in order to give a high confidence in the BHTE model (a typical value of $Q = Q_{min} = 0.1$ was chosen). In voxel #1, close to the focal point, accurate results with an improved precision could be visually observed, as shown in Fig. 4a: While the original measured temperature shows up to $5\,^{\circ}\mathrm{C}$ of temporal variation between two successive acquisitions, it remained stable over the whole experiment using the EKF approach. The precision

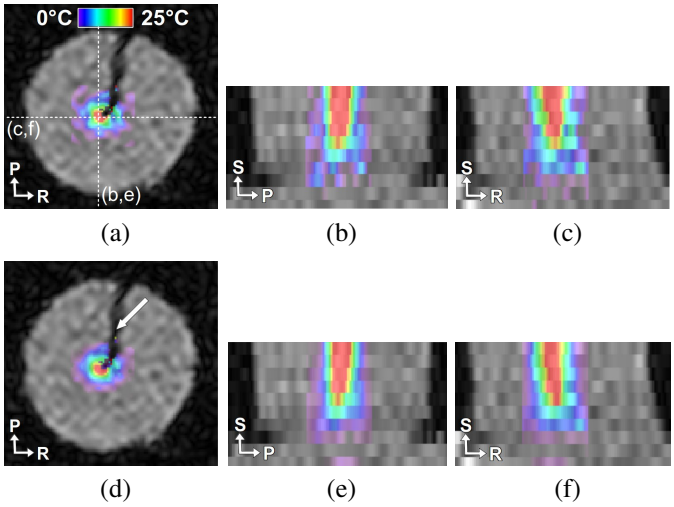

Fig. 1: MR-Thermometry results obtained on the phantom heating experiment with HIFU. Temperature maps are displayed along the three directions of the space, across the center of the focal point, after 30 seconds of heating. (a), (b) and (c) show the original spatio-temporally under-sampled measured MR-temperature maps. (d), (e) and (f) show the AEKF reconstructed temperature data. (a-d), (b-e) and (c-g) display coronal, sagittal and transversal directions, respectively. The read (R), phase (P) and slice (S) directions are reported on the bottom left of each image.

of the MR thermometry was quantified during the cool-down period (time interval $120-280$ s) using the standard deviation between MR measurements and a fitted exponential decay curve, and was improved from an original value of $0.9\,^{\circ}\mathrm{C}$ to $0.11\,^{\circ}\mathrm{C}$ using the additional a priori knowledge of the system physics provided by the BHTE. However, it can be observed in Fig. 4b that results were found to be less accurate in voxel #2, which was located in the periphery of the focal point.

Then, we applied the proposed heuristic for the dynamic update of Q on a voxel-by-voxel basis. The temporal evolution of the estimated temperature bias ϵ_t is reported for the two examined voxels in Fig. 5. Concerning voxel #1, the time period with $\epsilon > \epsilon_{threshold}$ covers a duration of ~ 2 seconds (which represents less than 1% of the total experiment time). It can also be observed that, in this voxel, the model is found to be accurate most part of the time, except when the sonication is stopped. The time period with $\epsilon > \epsilon_{threshold}$ was found to be equal to ~ 30 seconds for voxel #2 (which represents $\sim 11\%$ of the total experiment time). Although the model accuracy decreases strongly upon start of the sonication, the model was found to be accurate in the cool down period. Fig. 6 shows the impact of the process noise covariance Q adaptation on the EKF reconstructed temperature data: The temperature evolution measured in voxel #2 was improved compared to results shown in Fig. 4b.

The inserts of Fig. 4 and Fig. 6 display the effect of the temporal interpolation of the applied AEKF: Although the temperature information was updated only every 9^{th} acquisition cycle, a continuous estimation was available for all

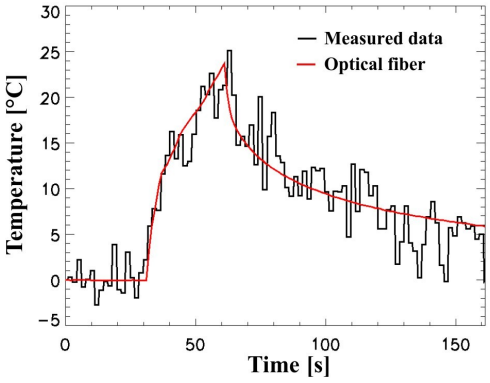

(a)

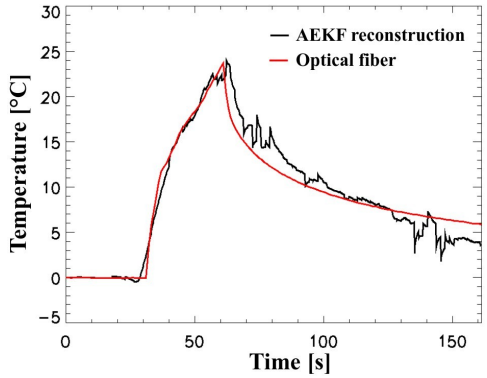

(b)

Fig. 2: Comparison between the PRF-based MR-thermometry (black line) and the reference temperature measured with the thermocouple probe (red line). (a): with the original spatio-temporally under-sampled measured MR-temperature, (b): with the AEKF reconstructed temperature data.

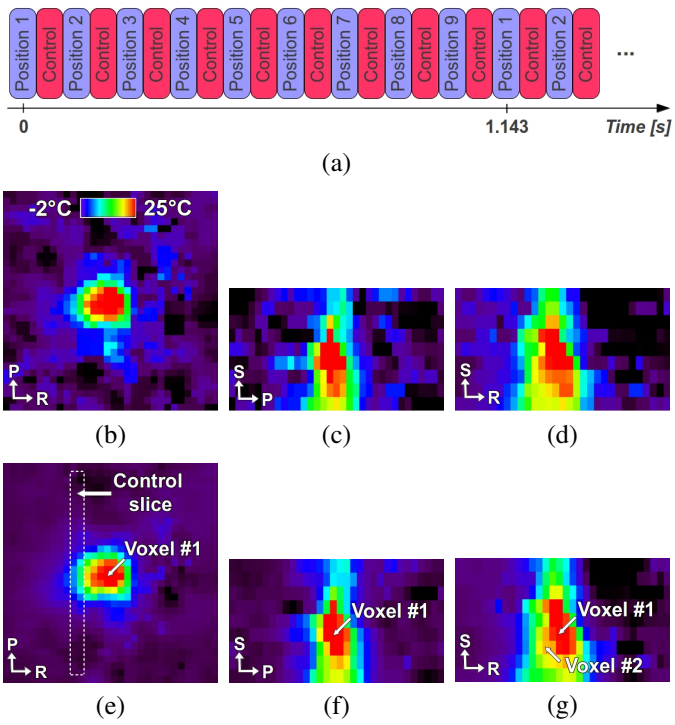

(a) (b) (c) (d) (e) (f) (g)

Fig. 3: MR-Thermometry results obtained on a pig kidney during HIFU ablation. The acquisition timing diagram is detailed in (a): The coronal slice, which sweeps continuously through nine positions, is indicated in blue, while the static sagittal control slice is reported in red. Temperature maps are displayed along the three directions of the space, across the center of the focal point, after 50 seconds of HIFU heating of a porcine kidney: (b), (c) and (d) show the original spatio-temporally under-sampled measured MR-temperature maps, (e), (f) and (g) show the AEKF reconstructed temperature data. The position of the control slice is shown in (e).

time points, which showed, compared to the measured data, a significantly reduced measurement noise.

The estimated temperature bias ϵ_t was found to be maximal during the HIFU energy deposition period. Fig. 7 shows the spatial distribution of the maximal temperature bias ϵ_t reached during the experiment for each voxel of the observed field of view. Although very high ϵ_t values ($> 3\,^{\circ}\mathrm{C}$) were observable in voxels prone to low MR-signal, ϵ_t remained well below $2.5\,^{\circ}\mathrm{C}$ in the heated region.

The efficiency of both the sliding window-based and the AEKF reconstruction is evaluated in Fig. 8, using temperature informations of the control slice as a reference. In order to account for the different slice geometries, a spatial temperature average was performed over four neighboring voxels (for the control slice as well as for the reconstructed temperature volume) to compare the temperature in voxels with an identical isotropic resolution (i.e. $6 \times 6 \times 6$ mm^3). The temperature evolution is reported in a single voxel located in the heated region, which is present both in the control slice and in the reconstructed volumes. While a similar accuracy was obtained with the sliding window-based and the AEKF reconstruction (an average temporal temperature difference of about $0.1\,^{\circ}\mathrm{C}$ was measured), the precision was improved (the standard deviation of temperature difference was found to decrease from an initial value of $1.2\,^{\circ}\mathrm{C}$ to below $0.6\,^{\circ}\mathrm{C}$), as shown in the inserts of Fig. 8.

Less than 15 milliseconds were required for the complete calculation of one reconstructed 3D volume on our computational platform. This rendered the method compatible with sub-second MRI and the sampling frequency was only limited by the MR-acquisition time (up to 16 Hz was achievable with the used MR-imaging protocol). The latency (i.e the delay between the actual time of the measurement and the availability of the information) is equal to the sum of the remaining acquisition time after the passage of the k-space center (equal to half of the echo time with the used MR-imaging protocol), the data transport duration (which was evaluated to be approximatively equal to 10 milliseconds with the used implementation) and the image processing time. A latency lower than 60 milliseconds was thus achievable for the obtention of one 3D temperature volume with the proposed AEKF reconstruction.

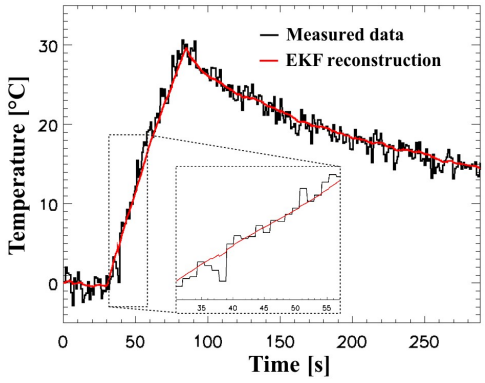

(a)

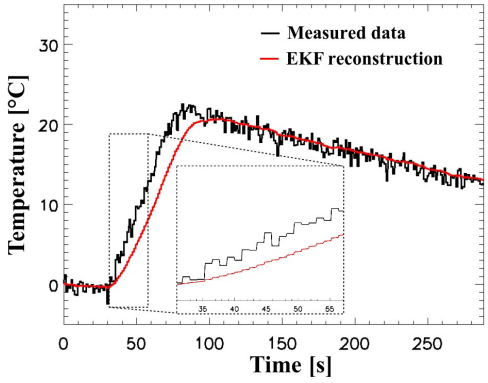

(b)

Fig. 4: Temporal temperature evolution obtained with a fixed Q value (we choose $Q = 0.1$ in order to give a high confidence in the BHTE model). (a): in a single voxel located close to the focal point area (voxel $\#1$ in Fig. 3), (b): further in the vicinity of the focal point (voxel $\#2$ in Fig. 3). The black curve shows the measured MR-temperature data, while the red curve depicts the volumetric EKF reconstructed temperature data. Note the significant reduction in measurement noise obtained with the EKF reconstruction in (a), and the loss of accuracy in (b).

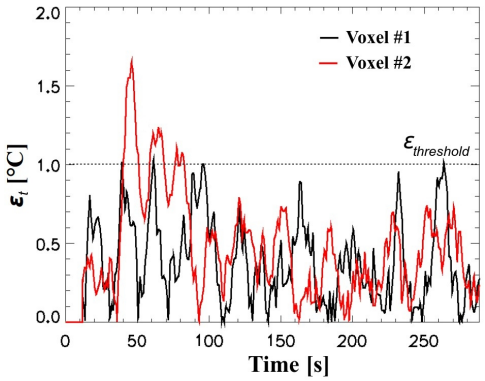

Fig. 5: Temporal evolution of the estimated temperature bias ϵ_t in the two voxels reported in Fig. 3): voxel $\#1$ (black line) and voxel $\#2$ (red line).

IV. DISCUSSION

The method extends our recent work reported in [24] to reconstruct continuous volumetric temperature data from spatio-temporally under-sampled 3D MR-temperature maps using an Extended Kalman Filter (EKF). The bio-heat transfer equation

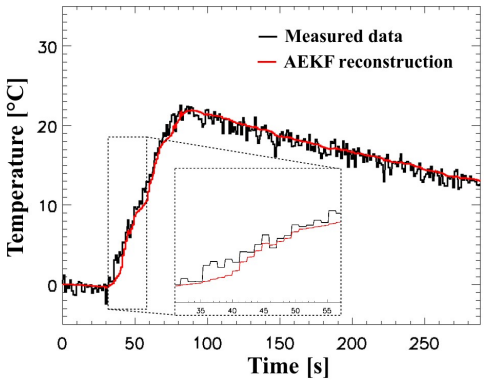

Fig. 6: Temporal temperature evolution obtained with a dynamic voxel-by-voxel basis Q adaptation in voxel $\#2$ (arrow (2) in Fig. 3b). Note the improvement of the reconstruction at the beginning of the heating process, as compared to the scenario reported in Fig. 4b in which to Q was not dynamically adapted.

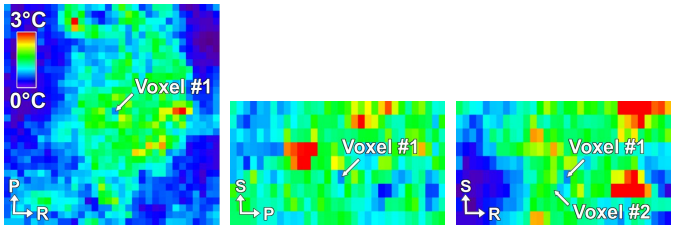

(a) (b) (c)

Fig. 7: Spatial distribution of the maximal temperature bias ϵ_t reached in each voxel during the porcine kidney experiment. (a), (b) and (c) display coronal, sagittal and transversal directions, respectively.

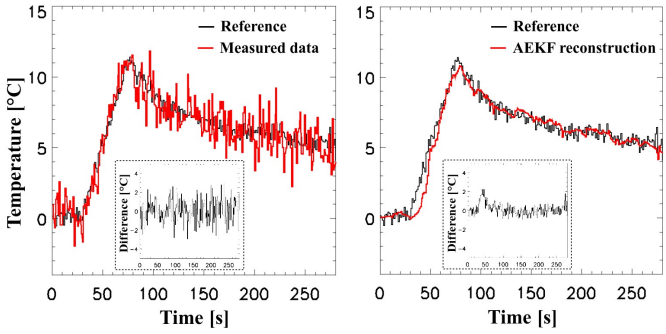

(a) (b)

Fig. 8: Accuracy of the proposed reconstruction evaluated using the temperature measured in the control slice as a reference. The temporal temperature evolution in the heated region obtained from the measured (a) and the AEKF reconstructed temperature data (b) are compared to the reference provided by the control slice. Note, in the inserts, the significant reduction in measurement noise obtained with the AEKF reconstruction while maintaining an identical averaged accuracy.

(BHTE) was employed as the model for 3D temperature prediction, which includes the applied acoustic power, a priori knowledge of the absorption rate, the heat diffusion coefficient and the perfusion value.

The proposed method is a step toward a precise volumetric MR-temperature monitoring with a high spatial and temporal resolution. Since all measured temperature values are Kalman filtered using a predictor which models the underlying energy deposition and heat evacuation processes, the measurement noise is reduced. It is in particular important to note that this increase in thermometric precision may have a direct impact on the accuracy of the estimation of the tissue necrosis, since the calculation of the thermal dose is based on a temporal integration of the temperature on a voxel-by-voxel basis [6].

Since the BHTE models the physical processes of heat diffusion and absorption, it requires to be applied in 3D space in order to obtain unbiased results. However, the available acquisition time is generally too limited in interventional imaging applications to obtain full 3D thermometric coverage of the heated area, especially if physiological motion has to be resolved. As a consequence, previous approaches [24], applied the BHTE to 2D or severely undersampled 3D datasets, which leads to a systematic under-estimation of the heat evacuation and neglects heat inflow from adjacent slices, in particular for low temporal imaging resolution. This led to a systematic accuracy bias introduced to the filtering process. In the presented approach, the targeted area was continuously scanned during the heating process by a multi-slice sequence and thus a 3D implementation of the BHTE model was possible, which improved the filtering performance in terms of both accuracy and precision.

For the *in-vivo* experiment, the proposed method allowed the reconstruction of thermometric 3D datasets with an interpolated temporal resolution of 0.127 s from a spatio-temporally under-sampled data (update time per voxel 1.143 s) in a temporally consistent way: Although neighboring voxels in slice direction are in the original dataset 0.127 s apart, all voxels in the 3D map show the temperature evolution at the same point in time.

The computation times for the reconstruction of a complete 3D volume were found to be below the acquisition time of one single slice (63.5 ms on the *in-vivo* experiment). In addition, compared to the previously proposed approach for 3D dynamic temperature reconstruction [27], only the knowledge of past temperature measurements is required, which renders the method compatible with a real-time implementation.

The intrinsic limit of the proposed approach arises from its dependence on a correct representation of the underlaying heating process by the BHTE model. The parameters of the BHTE model, which are in practice often not exactly known, and are subjected to spatio-temporal changes due to the heating process. Furthermore, although the acoustic field can be precisely modeled in homogeneous media, variations in the celerity and attenuation will generally modify the predicted field in biological tissue. As a consequence, the estimate based on Rayleigh integration was sufficient for accurate filtering directly in the focal point area (see Fig. 4a), but was found inaccurate in the periphery of the focus, leading to a systematic underestimation of the observed temperature (see the insert of Fig. 4b).

These model errors can lead to a systematic accuracy bias, which could be observed when Q was fixed deliberately to give a high confidence to the BHTE model, as reported in Fig. 4. In the proposed approach, this loss of accuracy was addressed by the dynamic model covariance adaptation of the EKF, which applies a stronger weighting to the measured data in the affected regions. For this purpose, the adjustment of the Q parameter allowed handling correctly the model accuracy in the proposed filter: While high Q values lead to measurement fidelity, low Q values lead to an emphasis on modeling. Although this reduces the achievable noise removal, it prevents the filtering to introduce a systematic bias and thus a loss of accuracy in the affected regions. In the scope of the presented work, the numerical complexity induced by the increased amount of data in 3D prevented the use of an iterative optimization scheme to find the optimal Q minimizing the filter accuracy ϵ_t as it was proposed in [24]. Instead, a simple heuristic was introduced which allowed an adaptation of Q on a voxel-by-voxel basis based on an a priori error estimate of the process noise covariance.

Another important aspect is the latency of the Q adaptation process: In the presented implementation, this latency was determined by the size of the temporal window employed to evaluate the filter accuracy ϵ_t (which covered the past 10 seconds in the presented *in-vivo* study). Although a high temporal window size increases the precision of the evaluation, it also increases the latency of the filter adaptation. This latency may disturb the AEKF reconstruction by raising the two following scenarios:

- In the focal point, the estimated model accuracy can be biased when the HIFU generator was shifted from ON to OFF (the estimated model accuracy reached the maximal allowed threshold ϵ_t, as shown on Fig. 1 and Fig. 5).
- In the vicinity of the focal point, it typically introduces a delay in the EKF adaptation at the beginning of the HIFU sonication, as it can be observed in Fig. 6 and Fig. 8b.

With the proposed approach, the high temporal resolution per volume associated with a low latency allowed for a typical non-invasive measurement of the local temperature distribution, which is of particular interest for highly perfused and/or mobile organs targets such as kidney and liver tumors [18]. As a consequence, the current approach is a step toward an adequate spatial resolution over 3D volume with sufficient temporal resolution to cope with sophisticated tumor ablation procedures which involves high energy depositions, real-time feedback control, and offline optimized 3D trajectory. However, for this purpose, several limitations will need to be addressed in future studies:

First, future works must involve the integration of a 3D acoustic pressure field simulation accounting for media with heterogeneous acoustic properties in the beam path [32]. Although a Fourier-based approach could be used in the scope of the current study to speed up the on-line BHTE model resolution [31] (see Eq. (2)), this technique is only valid under the assumption that no heterogeneous media are present. The solution of the BHTE in heterogeneous media requires more

complex numerical solutions which would potentially render a real-time volumetric AEKF reconstruction challenging.

Second, the implemented BHTE must be improved by integrating several physiological parameters into the model: One limitation of the implemented predictor model arises from the negligence of the heat evacuation due to tissue perfusion. Future works on *in-vivo* tissue, especially in the liver, will require a careful assessment of the corresponding error bias and potentially to take the perfusion term in Eq. (1) into account. Similarly, an assessment of the local absorption and diffusion also needs to be achieved. The a priori knowledge of these parameters is in practice difficult and often relies either on empirical data or calibration experiments [7]. Moreover, although apparent coefficients can be expected to be sufficiently homogeneous within large organs such as the liver, this assumption could break down in smaller heterogeneous organs such as the kidney, or close to organ boundaries, where both become spatially variant. An accurate assessment of these parameters will improve the performance of the volumetric reconstruction by enhancing the BHTE performances, which, in turn, will reduce the need of large scale Q adaptations. The latter needs to be limited due the unavoidable Q adjustment process latency (see the delay of the correction and aliasing effects in the insert of Fig. 4b which are not completely removed by the proposed approach).

Finally, in order to take into account dynamic changes in the energy deposition and heat evacuation during the ablation (acoustic absorption, heat diffusion, tissue perfusion), the concept of volumetric sonications has been combined with retroactive feedback control of the HIFU power. However, an important challenge for HIFU ablations in organs in the upper abdomen arises from the fact that the respiratory cycle causes a continuous displacement of the target area. Therefore, the focal point of the HIFU-system must be adaptively repositioned as the organ moves with respect to the external transducer in order to avoid damaging healthy tissue and to limit acoustic energy losses. It has been demonstrated that the volumetric heating procedure can be combined with HIFU motion correction by compensating the tissue displacement for each short sonication period [33]. As a consequence, future work will also involve the integration of the correction of motion artifacts in thermal maps [34] [35], as well as the integration into the BHTE of an update of the focal point position combined with a trajectory optimized by the feedback control strategy.

V. CONCLUSION

The proposed approach combined temperature measurements obtained from a spatio-temporally under-sampled multi-slice acquisition with a bio-heat transfer equation for the reconstruction of 4D MR-thermometry. Compared to the approach proposed previously [27], which is, in its current form, intrinsically limited to post-processing, the proposed EKF reconstruction is compatible with real-time processing and has been implemented so that the computation times for the reconstruction of a complete 3D volume were found to be below the acquisition time of one single slice, associated with a short latency.

The resulting increased spatial coverage and temporal resolution may facilitate real-time feedback control strategies, which can be based on either the temperature or the thermal dose, depending on the particular application scenario. For HIFU applications, this allows maximizing the energy deposition in the targeted area while reducing undesired heating in the near-field. Hence, the described method is a step towards effective tumor ablations while inflicting minimal damage on the healthy surrounding tissue.

ACKNOWLEDGMENT

The author would like to thank the European Research Council (project ERC-2010-AdG-20100317, Sound Pharma) and the Foundation InNaBioSanté (project ULTRAFITT) for funding.

REFERENCES

[1] B. Denis de Senneville, B. Quesson, and C. T. W. Moonen, "Magnetic resonance temperature imaging," *International Journal of Hyperthermia*, vol. 21(6), pp. 515–531, 2005.

[2] V. Rieke and K. B. Pauly, "MR thermometry," *Journal of Magnetic Resonance Imaging*, vol. 27(2), pp. 376–390, 2008.

[3] J. Hindley, W. M. Gedroyc, L. Regan, E. Stewart, C. Tempany, K. Hynyen, N. Mcdannold, Y. Inbar, Y. Itzchak, J. Rabinovici, H. Kim, J. F. Geschwind, G. Hesley, B. Gostout, T. Ehrenstein, S. Hengst, M. Sklair-Levy, and F. Shushan, A. Jolesz, "MRI guidance of focused ultrasound therapy of uterine fibroids: early results," *AJR Am J Roentgenol*, vol. 183(6), pp. 1713–1719, 2004.

[4] G. D. Dodd, M. C. Soulen, R. A. Kane, T. Livraghi, W. R. Lees, Y. Yamashita, A. R. Gillams, O. I. Karahan, and H. Rhim, "Minimally invasive treatment of malignant hepatic tumors: at the threshold of a major breakthrough," *Radiographics*, vol. 20(1), pp. 9–27, 2000.

[5] R. J. Stafford and J. Hazle, "Magnetic resonance temperature imaging for focused ultrasound surgery: a review," *Top Magn Reson Imaging*, vol. 17(3), pp. 153–63, 2006.

[6] S. A. Sapareto and W. C. L. Dewey, "Thermal dose determination in cancer therapy," *Int J Radiation Oncology Biol Phys*, vol. 10, pp. 787–800, 1964.

[7] C. Mougenot, B. Quesson, B. Denis de Senneville, P. de Oliveira, S. Sprinkhuizen, J. Palussière, N. Grenier, and C. T. W. Moonen, "Three-dimensional spatial and temporal temperature control with MR thermometry-guided focused ultrasound (MRgHIFU)," *Magnetic Resonance in Medicine*, vol. 61, pp. 603–614, 2009.

[8] R. Deckers, B. Quesson, J. Arsaut, S. Eimer, F. Couillaud, and C. T. W. Moonen, "Image-guided, non-invasive, spatiotemporal control of gene expression," *Proc Natl Acad Sci U S A*, vol. 106, pp. 1175–1180, 2009.

[9] T. Conturo and G. Smith, "Signal to noise in phase angle reconstruction: Dynamic range extension using phase reference offsets," *Magnetic Resonance in Medicine*, vol. 15, pp. 420–437, 1990.

[10] C. T. W. Moonen, G. Liu, P. van Gelderen, and G. Sobering, "A fast gradient-recalled MRI technique with increased sensitivity to dynamic susceptibility effects," *Magnetic Resonance in Medicine*, vol. 26, pp. 184–189, 1992.

[11] K. P. Pruessmann, M. Weiger, M. B. Scheidegger, and P. Boesiger, "SENSE: sensitivity encoding for fast MRI," *Magnetic Resonance in Medicine*, vol. 42, pp. 952–962, 1999.

[12] D. K. Sodickson and W. J. Manning, "Simultaneous acquisition of spatial harmonics (SMASH): fast imaging with radiofrequency coil arrays," *Magnetic Resonance in Medicine*, vol. 38, pp. 591–603, 1997.

[13] B. Madore, G. H. Glover, and N. J. Pelc, "Unaliasing by Fourier-encoding the overlaps using the temporal dimension (UNFOLD), applied to cardiac imaging and fMRI," *Magnetic Resonance in Medicine*, vol. 42, pp. 813–828, 1999.

[14] J. Tsao and P. Boesiger, "k-t BLAST and k-t SENSE: dynamic MRI with high frame rate exploiting spatio temporal correlations," *Magnetic Resonance in Medicine*, vol. 50, pp. 1031–1042, 2003.

[15] D. Daum, N. Smith, R. King, and K. Hynynen, "In vivo demonstration of noninvasive thermal surgery of the liver and kidney using an ultrasonic phased array," *Ultrasound Med. Biol.*, vol. 25, pp. 1087–1098, 1999.

[16] D. Kopelman, Y. Inbar, A. Hanannel, G. Dank, D. Freundlich, A. Perel, D. Castel, A. Greenfeld, T. Salomon, M. Sareli, A. Valeanu, and M. Papa, "Magnetic resonance-guided focused ultrasound surgery (MRgFUS). four ablation treatments of a single canine hepatocellular adenoma," *HPB (Oxford)*, vol. 8, pp. 292–298, 2006.
[17] M. Ries, B. Denis de Senneville, S. Roujol, Y. Berber, B. Quesson, and C. T. W. Moonen, "Real-time 3D target tracking in MRI guided focused ultrasound ablations in moving tissues," *Magnetic Resonance in Medicine*, vol. 64(6), pp. 1704–1712, 2010.
[18] S. Roujol, M. Ries, B. Quesson, C. T. W. Moonen, and B. Denis de Senneville, "Real-time MR-thermometry and dosimetry for interventional guidance on abdominal organs," *Magnetic Resonance in Medicine*, vol. 63, no. 4, pp. 1080–7, 2010.
[19] C. Damianou and K. Hynynen, "Focal spacing and near-field heating during pulsed high temperature ultrasound therapy," *Ultrasound Med.Biol.*, vol. 19(9), pp. 777–787, 1993.
[20] C. Mougenot, M. Kohler, J. Enholm, B. Quesson, and C. Moonen, "Quantification of near-field heating during volumetric MR-HIFU ablation," *Med Phys*, vol. 38(1), pp. 272–282, 2011.
[21] B. Quesson, C. Laurent, G. Maclair, B. Denis de Senneville, C. Mougenot, M. Ries, T. Carteret, A. Rullier, and C. T. W. Moonen, "Real-time volumetric MRI thermometry of focused ultrasound ablation in vivo: a feasibility study in pig liver and kidney," *NMR in Biomedicine*, vol. 24(2), pp. 145–153, 2011.
[22] G. Ye, P. Smith, and J. Noble, "Model-based ultrasound temperature visualization during and following HIFU exposure," *Ultrasound Med Biol*, vol. 36(2), pp. 234–249, 2010.
[23] N. Todd, A. Payne, and D. Parker, "Model predictive filtering for improved temporal resolution in mri temperature imaging," *Magnetic Resonance in Medicine*, vol. 63, pp. 1269–1279, 2010.
[24] S. Roujol, B. Denis de Senneville, S. Hey, C. Moonen, and M. Ries, "Robust Adaptive Extended Kalman filtering for real time MR-thermometry guided HIFU interventions," *IEEE Transaction on Medical Imaging*, vol. 31(3), pp. 533–542, 2012.
[25] R. Kalman, "A new approach to linear filtering and prediction problems," *Journal of Basic Engineering*, vol. 82(2)1, pp. 35–45, 1960.
[26] N. Todd, G. Adluru, A. Payne, E. DiBella, and D. Parker, "Temporally constrained reconstruction applied to MRI temperature data," *Magnetic Resonance in Medicine*, vol. 62(2), pp. 406–419, 2009.
[27] N. Todd, U. Vyas, U. J. de Bever, A. Payne, and D. Parker, "Reconstruction of fully 3D high spatial and temporal resolution MR temperature maps for retrospective applications," *Magnetic Resonance in Medicine*, vol. 67(3), pp. 724–730, 2012.
[28] N. Todd, J. Prakash, H. Odeen, J. de Bever, A. Payne, P. Yalavarthy, and D. L. de Parker, "Towards real-time availability of 3-D temperature maps created with temporally constrained reconstruction," in *International Society for Magnetic Resonance in Medicine, 20th annual Meeting*, 2012.
[29] H. Pennes, "Analysis of tissue and arterial blood temperatures in the resting human forearm," *Journal of applied physiology*, vol. 1(2), pp. 93–122, 1948.
[30] C. Mougenot, L. Kabongo, B. Quesson, and C. T. W. Moonen, "MRgHIFU: Feedback temperature control with automatic deduction of BHT tissue parameters," *8th International Symposium on Therapeutic Ultrasound*, vol. 1113, pp. 231–235, 2009.
[31] B. Quesson, F. Vimeux, R. Salomir, J. de Zwart, and C. T. W. Moonen, "Automatic control of hyperthermic therapy based on real-time Fourier analysis of MR temperature maps," *Magnetic Resonance in Medicine*, vol. 47(6), pp. 1065–1072, 2002.
[32] V. A. Khokhlova, S. M. Bobkova, and L. R. Gavrilov, "Focus splitting associated with propagation of focused ultrasound through the rib cage," *Acoustical Physics*, vol. 56(5), pp. 665–674, 2010.
[33] B. Denis de Senneville, C. Mougenot, and C. Moonen, "Real time adaptive methods for treatment of mobile organs by MRI controlled high intensity focused ultrasound," *Magnetic Resonance in Medicine*, vol. 57(2), pp. 319–330, 2007.
[34] J. De Poorter, C. De Wagter, Y. De Deene, C. Thomson, F. Stahlberg, and E. Achten, "The proton resonance frequency shift method compared with molecular diffusion for quantitative measurement of two dimensional time dependent temperature distribution in phantom," *Journal of Magnetic Resonance Imaging*, vol. 103, pp. 234–241, 1994.
[35] B. Denis de Senneville, M. Ries, G. Maclair, and C. Moonen, "MR-guided thermotherapy of abdominal organs using a robust PCA-based motion descriptor," *IEEE Transaction on Medical Imaging*, vol. 30(11), pp. 1987–1995, 2011.